scientific reports

Check for updates

OPEN

Early-warning method for rock bursts based on the fractal characteristics of microseismic source

Yunlong Wu[1], Zhijie Zhu[1]✉, Kun Chen[2] & Fei Lv[2]

Mine disasters occur frequently during deep coal-mining operations in China; however, current monitoring and early-warning methods for rock bursts remain insufficient. To address this, this paper proposes an early-warning method for rock bursts based on the fractal dimension of microseismic energy. Through the establishment of an integral expression relationship between microseismic energy and fractal dimension, the spatio-temporal distribution characteristics of microseismic events are analyzed, revealing the precursor patterns of rock bursts. The results indicate that prior to the occurrence of a rock burst, parameters such as microseismic energy, event frequency, and fractal dimension all exhibit significant precursor characteristics. Furthermore, the temporal evolution of the fractal dimension can be divided into four distinct stages: stable, early-warning, deformation, and re-stabilization periods. This method provides a new approach for the quantitative early warning of rock bursts.

Keywords Rock burst, Fractal dimension, Surrounding-rock damage, Early warning, Precursor characteristics

In coal mining, the mechanisms underlying the formation and occurrence of rock bursts are highly complex; thus, controlling or preventing rock bursts is challenging. Monitoring and early warning play a critical role in prevention and mitigation efforts. Existing warning methods across various monitoring systems have achieved notable progress, and techniques such as microseismic monitoring, ground noise detection, stress measurement, and electromagnetic radiation monitoring have become widely adopted.

Excavation at the working face disturbs the surrounding rock, which, in its natural state, is prone to fracture development. During this process, elastic waves are released and can be detected by sensors. In mine engineering, such signals are referred to as microseismic events[1]. Microseismic monitoring provides a microscopic perspective for predicting, preventing, and controlling rock bursts in deep mines. Microseismic monitoring and early-warning methods have been investigated from different perspectives. Li[2–4] et al., based on damage mechanics theory, obtained detailed structural characteristics related to coal-rock damage and the variation patterns of microseismic energy events at different loading stages; Liu[5] et al. investigated the influence of coal pore structure and fractal characteristics, finding that the fractal dimension of each coal sample increased linearly with the number of liquid nitrogen freeze–thaw cycles; Li[6] conducted photographic and acoustic emission monitoring of fiber-reinforced concrete to study its characteristics such as compressive energy absorption, crack evolution, and fracture surface fractality. The more intact the specimen surface at failure, the lower its fractal dimension, which increased by 0.2–0.4 as surface fragmentation increased.

Although these studies have provided valuable insights into microseismic precursor information and its role in rock burst prediction, research on establishing quantitative standards for monitoring and early-warning systems remains limited. This limitation is addressed in the present study by applying fractal theory to analyze microseismic signal data obtained from a mine-monitoring and early-warning system.

The concept of fractal dimension was first proposed by a German mathematician named Felix Hausdorff in 1918, and fractal geometry was later introduced by a French mathematician named Benoît Mandelbrot in 1975[7]. Xie[8] introduced fractal geometry into the field of geotechnical engineering by examining its applications to rock fragmentation, damage, and fracture processes and the roughness of rock joint surfaces. Liu[9] conducted experimental analysis to demonstrate that the roughness curves of rock fracture surfaces exhibit self-similar

[1]School of Mining, Liaoning Technical University, Fuxin, China. [2]Shaanxi Huabin Yadian Coal Industry Co., Xianyang, China. ✉email: zhuzhijie@lntu.edu.cn

fractal characteristics and proposed a correspondence between fractal dimension values and the microscopic damage mechanisms of rocks. Qian et al.[10] applied fractal rock mechanics theory to reveal the evolution of fractal dimensions throughout the process of progressive surrounding-rock damage leading to macroscopic deformation. These studies provide a theoretical foundation for applying fractal theory to the analysis of monitoring-data distribution characteristics.

In this study, three-dimensional microseismic-monitoring data obtained from a coal mine in Shaanxi were used. A fractal integral expression of the monitoring data was established by integrating surrounding-rock-damage theory with fractal theory. The cumulative energy, maximum energy, ratio of the maximum energy to the total energy, and event frequency during the period preceding a rock burst were analyzed. The temporal sequence patterns of precursor information related to rock burst occurrence were identified based on the aforementioned analysis. Furthermore, the distribution patterns of fractal dimensions were analyzed from a mechanistic perspective. The results of this study provide a reference framework for enhancing monitoring and early-warning systems in coal mines.

Project background

In a coal mine in Shaanxi Province, China, the main coal seam under extraction is the #4 seam that has an average thickness of 16.7 m. The seam has a gentle inclination of less than 5° and lies at a burial depth of 645.3–766.4 m. It exhibits a strong propensity for rock bursts. The ZF1409 working face, investigated in this study, is the sixth coal-mining panel within the district. It has a strike length of 1,600 m, recoverable length of 1,442 m, and dip length of 200 m. Coal pillars measuring 40–45 m in width are left between adjacent working faces, with the drainage roadway from the preceding face located within the coal pillar. The immediate roof of the ZF1409 working face consists of 32.4 m of siltstone, whereas the main roof, approximately 40 m above the seam, comprises 28.7 m of siltstone. During extraction, the thick hard sandstone sections of the roof undergo intense structural activity. As progressive damage develops within the overlying strata, stability gradually declines, eventually leading to fracture and instability. These conditions increase the likelihood of rock bursts and other dynamic hazards.

Microseismic monitoring provides insight into the internal condition of the rock mass because elastic waves released during coal and rock failure are recorded. It is one of the most effective methods for detecting rock dynamic hazards. The mine is equipped with an ARAMIS M/E microseismic monitoring system for regional monitoring. This system records vibration events with energies greater than 100 J across a frequency range of 0–150 Hz. Within the ZF1409 working face, six monitoring points are arranged in a diamond-shaped layout. In the 1409 belt roadway, two microseismic sensors and one vibration receiver are installed: the first sensor is located 300 m from the open-off cut, the second sensor is positioned 300 m further inby, and the vibration receiver is placed 400 m beyond the second sensor. In the 1409 return airway, three microseismic sensors are installed: the first is 400 m from the open-off cut, the second is 400 m further inby, and the third is 300 m beyond the second. This arrangement ensures that all microseismic activity within the rock strata of the ZF1409 working face remains within the effective monitoring range of the system. The layout of the working-face microseismic system is shown in Fig. 1.

Integral relationship between fractal dimension and microseismic energy

The fractal dimension is characterized by scale invariance and self-similarity and can be calculated using various methods, such as the correlation integral and box-counting methods. In this study, the fractal dimension is calculated using the correlation integral method, which quantifies the proportion and complexity of events within a given scale range. The location and magnitude of microseismic energy events reflect the internal failure state of the coal–rock mass. Applying fractal dimension analysis to microseismic energy data can help to identify the locations where failure of the surrounding rock at the working face occurs.

The integral expression for the fractal dimension of microseismic energy is derived from the microseismic energy dissipated during the failure of the surrounding rock. Let $P_1(\Delta l)$ represent the probability of damage occurring in the surrounding rock within range Δl and $P(l)$ represent the probability of no damage in the surrounding rock within range ; then,

$$P_1(\Delta l) = \lambda \Delta l \cdot e^{-\lambda \cdot \Delta l}; \tag{1}$$

$$P(l) = e^{-\lambda l}. \tag{2}$$

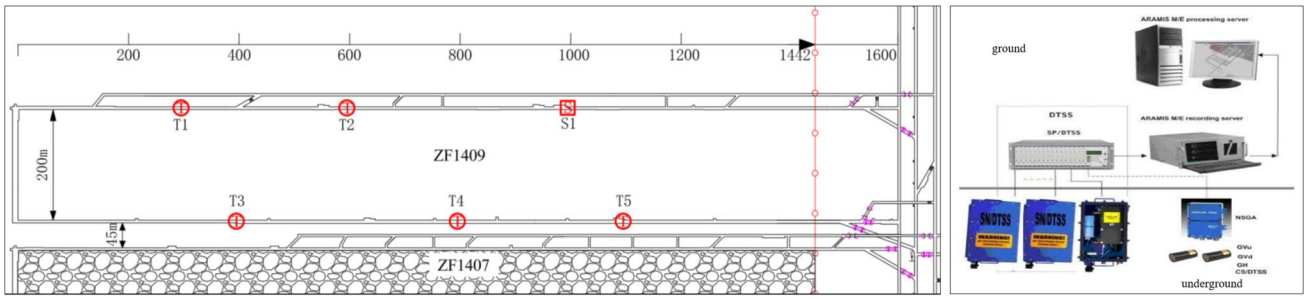

Fig. 1. Roadway layout and distribution of microseismic sensors at the working face.

The probability density of damage $\varphi(l)$ is

$$\varphi(l) = \frac{d\phi}{dl} = \lambda e^{-\lambda l}. \tag{3}$$

Let N denote the damage parameter (also referred to as the damage factor); then,

$$N = \frac{\int_0^x l\varphi(l)\,dl}{\int_0^\infty l\varphi(l)\,dl} = \frac{\frac{1}{\lambda}\left[-(\lambda l+1)e^{-\lambda l}\right]_0^x}{\frac{1}{\lambda}\Gamma(2)} = 1-(\lambda x+1)e^{-\lambda x}. \tag{4}$$

This formula can also be expressed in terms of α:

$$N = 1-\left(\frac{x}{\alpha}+1\right)exp\left[-\left(\frac{x}{\alpha}\right)\right]. \tag{5}$$

In a m-dimensional space ($m = 1, 2, 3$), generally

$$N = 1-\left[\left(\frac{x}{\alpha}\right)^m+1\right]exp\left[-\left(\frac{x}{\alpha}\right)^m\right]. \tag{6}$$

Here, α is the composite integrity, representing the average spacing of various damage events. It is a length-scale variable dependent on the external load. The larger the load, the smaller is α. The completeness α is a function of the load and must also be a function of deformation ε. In practice, α is considered to be inversely proportional to ε, i.e.

$$\alpha = \frac{c}{\varepsilon}, \tag{7}$$

where c is the scaling factor.

Let

$$\frac{x}{c} = \frac{1}{\varepsilon_0}. \tag{8}$$

Substituting Eq. (8) into Eq. (6) yields

$$N = 1-\left[\left(\frac{\varepsilon}{\varepsilon_0}\right)^m+1\right]exp\left[-\left(\frac{\varepsilon}{\varepsilon_0}\right)^m\right]. \tag{9}$$

When the stress in the surrounding rock reaches a certain threshold, any unit with a strength lower than that stress fails. The cumulative failure of these units leads to the macroscopic deterioration of the surrounding rock, which can be characterized as an increase in damage. The damage parameter (N) is a measure of the degree of material damage and is related to the number of failed units within the material. Accordingly, the relationship between the N and the probability density of unit failure is expressed in Eq. (9).

During the damage process of the surrounding rock, internal energy dissipation occurs. Xie[8] et al. defined energy damage as

$$N = \frac{E_d}{E_{cr}}, \tag{10}$$

where E_d is the energy dissipation value and E_{cr} is the critical energy dissipation value at which strength is lost. This constant is independent of the stress state and can be determined via the uniaxial compression testing of rocks. Loss of material strength occurs when $N = 1$ under any stress condition. The energy dissipation evolution equation can be obtained as

$$E_d = E_{cr}\left\{1-exp\left[-\left(\frac{\sigma}{\sigma_0}\right)^m\right]\right\}. \tag{11}$$

According to the schematic for monitoring energy dissipation during surrounding-rock damage shown in Fig. 2, the energy value monitored at point r is

$$E_r = E_d \times e^{-\alpha r}, \tag{12}$$

where α is the energy attenuation index and r is the distance of the energy point from the center of the monitored area.

Based on the principles of fractal geometry, the correlation integral of the volume distribution of the rock burst source can be expressed as

$$M_r = \frac{2M_a}{E_r(E_r-1)}, \tag{13}$$

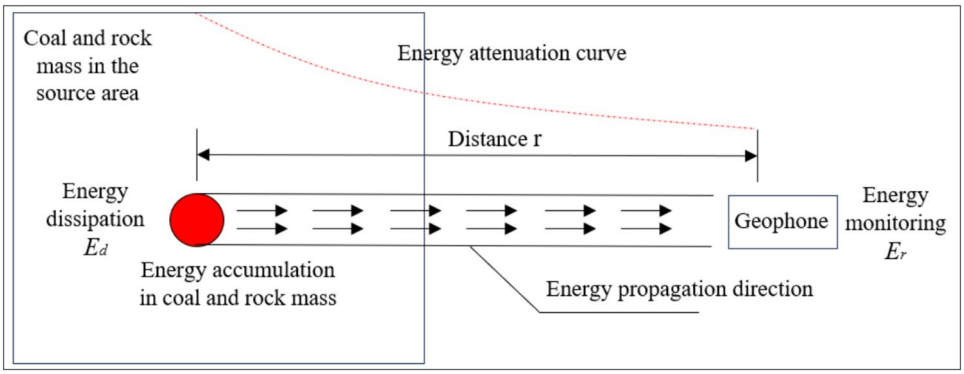

Fig. 2. Schematic for monitoring energy dissipation during rock damage.

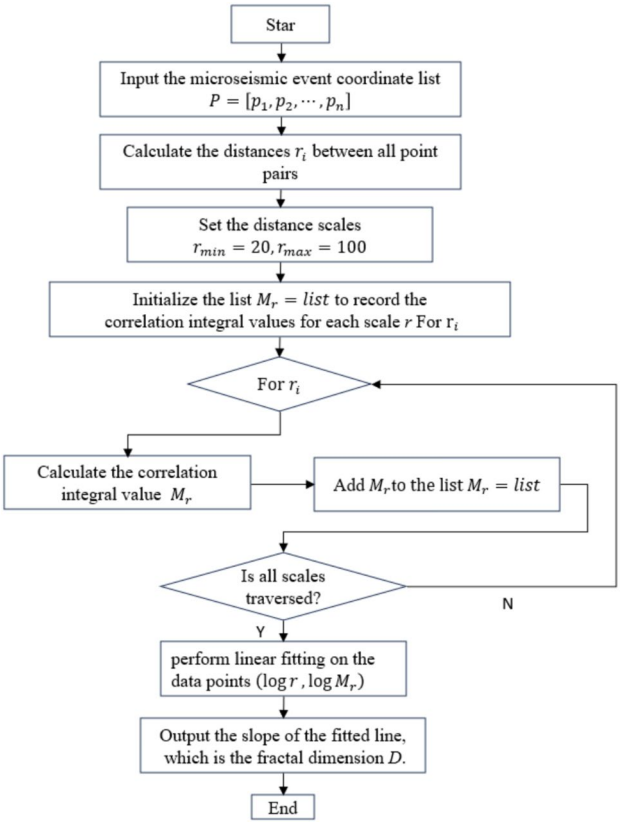

Fig. 3. Correlation Integral calculation process.

where M_a is the volumetric range energy of unit a.

When the energy generated during the damage process exhibits a fractal structure, the correlation integral of the monitored energy is expressed as

$$D = \lim_{r \to a} \frac{\lg M_r}{\lg r}. \tag{14}$$

That is, if the fitted curve of the fractal dimension (D) shows strong linear correlation, the microseismic energy during the development of damage in the surrounding rock at this stage has a fractal integral relationship. The corresponding computational procedure is illustrated in Fig. 3.

Characterization of microseismic activity

In this study, 11 months (April 2023–March 2024) of microseismic-monitoring data pertaining to the ZF1409 working face were analyzed; extraction commenced on April 12, 2023, and hydraulic fracturing of the roof

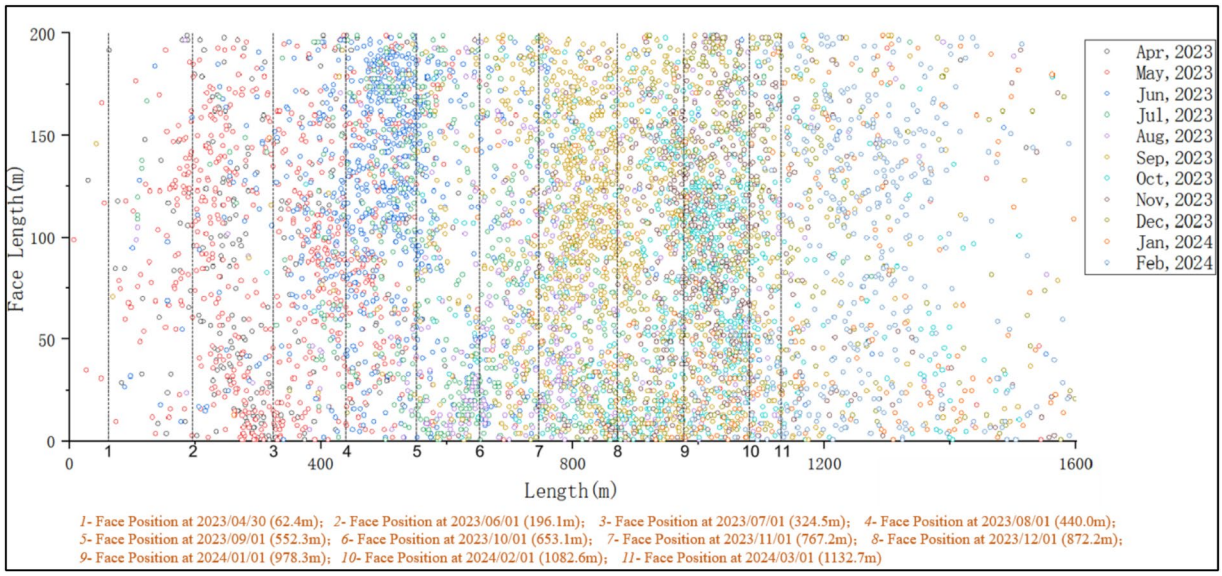

Fig. 4. Microseismic activity in different months.

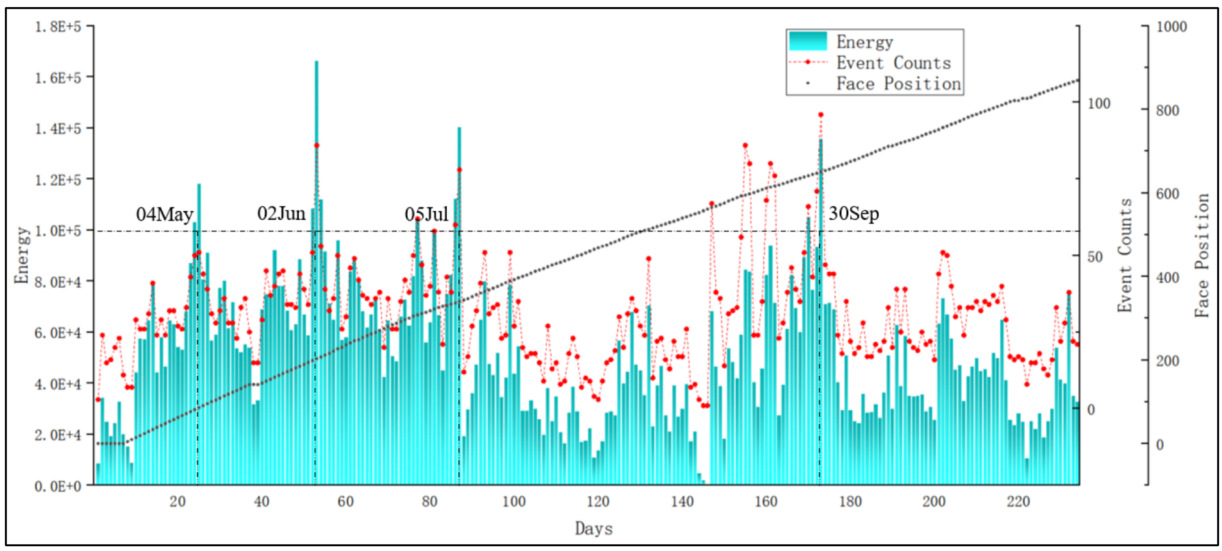

Fig. 5. Temporal variations in microseismic energy relative to the working-face position.

was performed in November 2023. An artificial filter was applied to remove noise from the raw dataset and to exclude events occurring outside the study area, which covered the working-face range of 1600 m × 200 m × 100 m. The monthly distribution of microseismic activity during the analysis period is shown in Fig. 4, where event clustering is clearly observed.

During the extraction process, the microseismic data collected over the statistical period were summarized, and the temporal variation of microseismic energy with respect to the working-face position is presented in Fig. 5. Based on the historical microseismic events recorded at the ZF1409 working face, it was observed that the daily cumulative energy exceeded 1×10^5 J in most rock burst cases. Consequently, this value was defined as the energy threshold for typical rock burst occurrences. Furthermore, this threshold aligns with the energy release levels observed in previous rock burst events within this mining area. To further examine precursor and post-event information, four parameters were analyzed: single-day cumulative energy, single-day maximum energy, event frequency, and ratio of the maximum energy to the total energy. Microseismic-monitoring results from more than one week prior to each rock burst were used to summarize the temporal variations in these indicators for the ZF1409 working face (Fig. 6). These results provide the basis for identifying the precursor characteristics of rock bursts.

Figures 5 and 6 reveal that in most cases, the daily cumulative energy of the working face remains below 105 J. Notably, monitoring data preceding rock burst events exhibit consistent precursor characteristics. Specifically,

approximately one week prior to an event, both the energy and frequency deviate significantly from normal levels. This deviation is manifested as frequent fluctuations in the event frequency, single-day maximum energy, and cumulative energy, with the magnitude of these fluctuations correlating with the cumulative energy at the time of the rock burst (Fig. 7).

Based on this analysis, the statistical characteristics of rock burst precursors are summarized in Table 1. In the week preceding a rock burst, the cumulative energy typically undergoes two fluctuations: a minimum value is observed 3–4 days before the event, followed by a gradual increase leading up to the rock burst. The highest recent peak in the maximum energy is observed 5–6 days before the event, whereas a lower peak is observed 3–4 days prior. The minimum event frequency appears 6–7 days before the event, with a secondary low 3–4 days prior. The peak ratio of the maximum energy to the total energy is noted 6–7 days before the rock burst, followed by a decreasing trend 2–4 days prior. These observations are consistent with findings reported in previous studies[11,12].

In the present analysis, deviation trends in microseismic-monitoring parameters for the early warning of rock bursts were initially classified based solely on typical rock burst events. However, during the extraction process, cases in which the daily cumulative event energy did not exceed the threshold of 1.0×10^5 J were observed; however, variations in the event frequency and energy release were comparable to, or greater than, those observed during typical events. Moreover, the statistical patterns identified were difficult to translate into quantitative criteria for the early warning of rock bursts. To address these limitations, the fractal dimension method was employed to enable quantitative prediction of rock burst occurrences.

Early-warning mechanism for deformation based on fractal dimension

Fractal-dimension measurement method

The spatial distribution of microseismic energy source points can be represented as a discrete point set, from which the fractal dimension describing the evolution of damage in the surrounding rock mass can be determined.

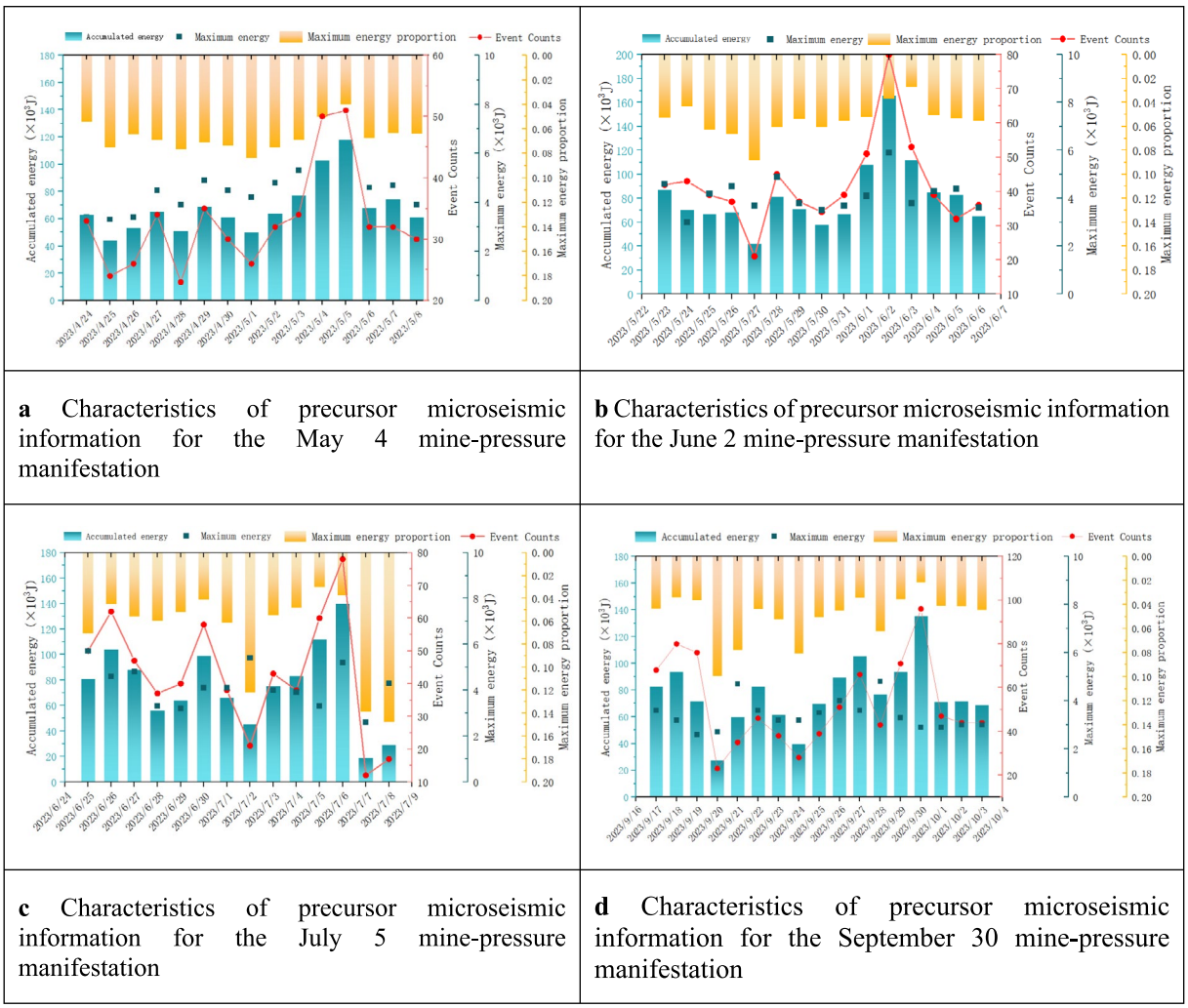

a Characteristics of precursor microseismic information for the May 4 mine-pressure manifestation

b Characteristics of precursor microseismic information for the June 2 mine-pressure manifestation

c Characteristics of precursor microseismic information for the July 5 mine-pressure manifestation

d Characteristics of precursor microseismic information for the September 30 mine-pressure manifestation

Fig. 6. Characteristics of precursor microseismic information for mine-pressure manifestations during extraction at the working face.

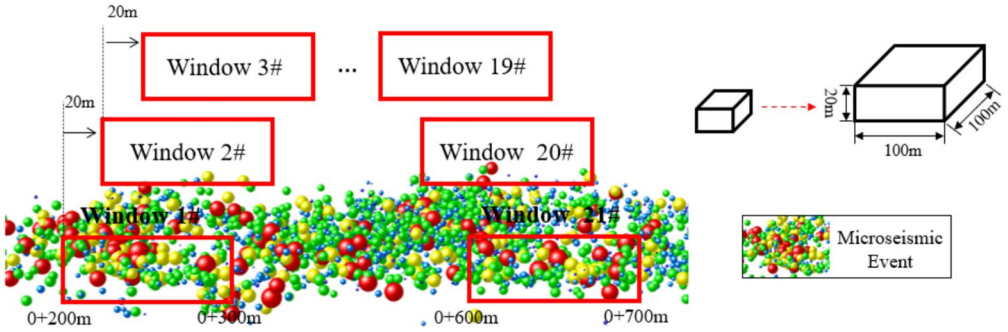

Fig. 7. Schematic for the sliding-overlay calculation of the rectangle window.

Type	Cumulative energy	Maximum energy	Frequency	Maximum energy proportion
Temporal precursor characteristics	Minimum values are observed approximately 3–4 days prior to the rock burst event, followed by a steady and progressive increase until the event occurs	The highest recent peak appears 5–6 days before the rock burst event, whereas lower values appear 3–4 days before the event	The minimum value is noted 6–7 days prior to the rock burst event, and lower values appear 3–4 days prior	Higher values are observed 6–7 days prior to the rock burst event, and lower values appear 3–4 days prior

Table 1. Statistical characteristics of the precursors of rock burst events.

Extensive research on fractal dimensions has been conducted worldwide, and the box-counting method has been widely recognized to be effective for fractal measurements. Consequently, the box-counting method is extensively employed to estimate the dimension of natural fractals. The relationship between the number of events and the radius in the box-counting method can be expressed as

$$M_r \propto r^D, \tag{15}$$

where M_r is the number of discrete bodies with characteristic size r, C is a constant, and D is the fractal dimension.

When employing a rectangle overlay approach with side lengths a, b, and c, the relationship between the energy contained within the volume and the side length of the rectangle can be expressed as

$$M_r \propto abc; \tag{16}$$

$$M_r \propto C_1 C_2 a^3. \tag{17}$$

If the distribution satisfies a fractal distribution, then

$$M_r = CC_1C_2 \cdot a^D. \tag{18}$$

Taking the logarithm of both sides of the equation yields

$$\lg M_r = \lg C + \lg C_1 + \lg C_2 + D\lg a, \tag{19}$$

where $\lg C$, $\lg C_1$, and $\lg C_2$ are constants and D is the fractal dimension, i.e., the value of the slope in double logarithmic coordinates of $\lg M_r - \lg a$.

During the extraction of the working surface, both the clustering intensity and spatial distribution of microseismic events vary at different stages. To account for this variability, a sliding rectangular window overlay method was used. In this approach, spatial sliding is first performed based on the energy of microseismic events to delineate risk zones. The microseismic event energies within each risk zone are then subjected to equally spaced sliding along either the time axis or the space axis to calculate the corresponding fractal dimensions. In this method, spatial sliding is first performed to delineate risk zones. Microseismic events within each risk zone are then analyzed by applying equally spaced sliding windows along either the time axis or the space axis to compute the corresponding fractal dimensions. This procedure enables early-warning analysis from both temporal and spatial perspectives; thus, a deformation early-warning model is established based on the spatio-temporal variations in the fractal dimension of microseismic energy. For the initial calculation window, the rectangular side lengths were set as $a = 20$ m, $b = 20$ m, and $c = 4$ m. The dimensions of the three sides were then increased proportionally (a:b:c = 5:5:1) until $a = 100$ m, $b = 100$ m, and $c = 20$ m were reached. After the calculation for the first window was completed, the window was slid forward along the working face (e.g., from 0 + 220 m to 0 + 320 m from the open cut), and the process was repeated until the window reached the end of the

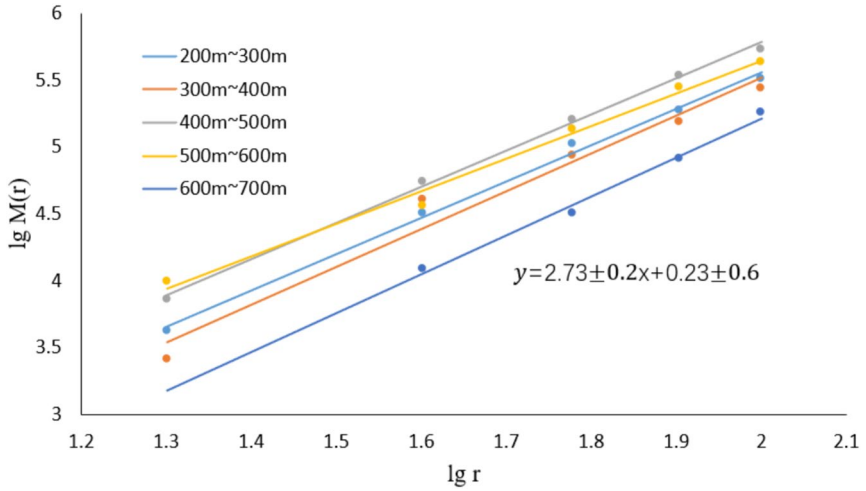

Fig. 8. Calculation results of energy-space fractal dimension.

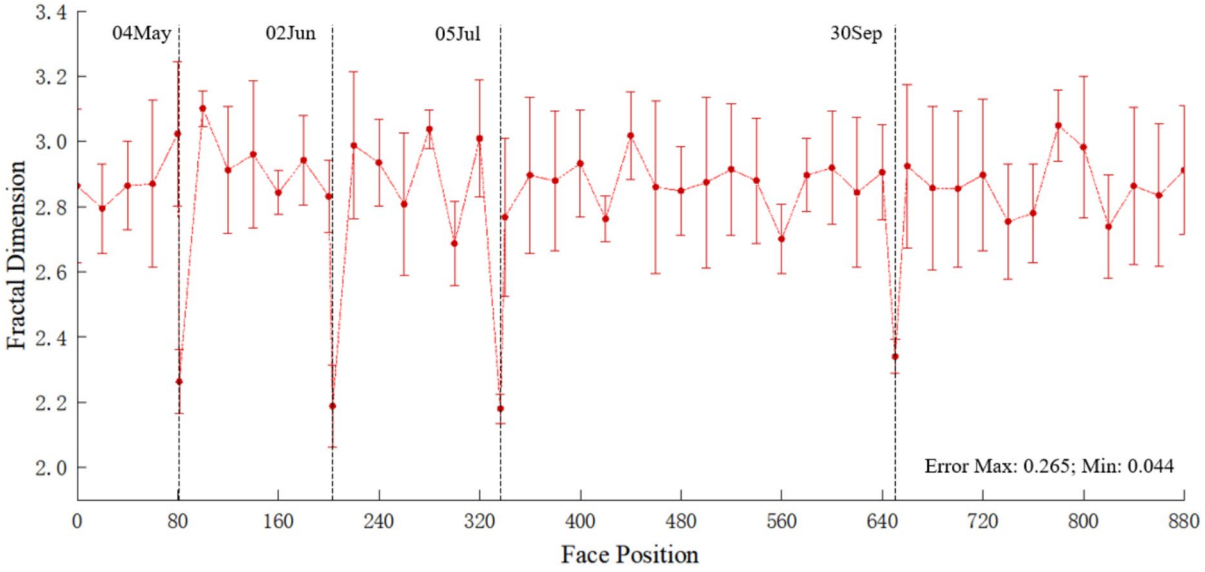

Fig. 9. Spatial variation curve of microseismic-energy fractal dimension.

face. For each window, the microseismic event energy (M_a) differed depending on window length a. Multiple sets of M_a values corresponding to different a values were obtained, and these data were fitted using linear regression and . The resultant $\lg M_a - \lg a$ curve in double-logarithmic space was used to determine the fractal dimensions for each calculation window. Plotting the fractal dimension values against the working-face position revealed the spatio-temporal evolution of microseismic energy.

Early warning of deformation based on spatial-scale fractal dimension

The $\lg M_a - \lg a$ relationship curves for the spatial distribution of microseismic event energy were plotted for each calculation window, and a linear fit was applied to each dataset. Five representative windows were selected, and their fitted curves for fractal dimension calculations are depicted in Fig. 8. As shown in Fig. 8, the sliding-window method using rectangle overlay produces a consistently strong linear relationship between $\lg M_a$ and $\lg a$ across all positions. This indicates that at the time of rock burst occurrence, the seismic source energy exhibits a spatial fractal distribution and a high degree of self-similarity.

The fractal dimension of microseismic events at the working face was calculated along the space axis, and its variation with the advance position of the working face is shown in Fig. 9. The spatial variation in the fractal dimension exhibits volatility, with average values of > 2.70. In relation to rock burst events, four notable instances of low fractal dimension values are observed: on May 4, at a working-face extraction position of 81.2 m during the initial weighting of the face, the fractal dimension of microseismic energy is 2.26; on June 2, at 203.1 m during the first weighting, the fractal dimension is 2.19; on July 5, at 336.6 m, periodic weighting causes large-

scale roof collapse, with a fractal dimension of 2.18; and on September 30, at 650.3 m, periodic weighting again causes large-scale roof collapse, with a fractal dimension of 2.34.

Lower fractal dimension values correspond closely to locations of rock burst occurrence. This phenomenon arises because insufficient void space behind hydraulic supports prevents large-scale collapse, resulting in higher roof stability. Under such conditions, the internal roof strata are less affected by primary in-situ stress, generating fewer microseismic events and higher overall fractal dimension values. When the fractal dimension decreases, energy originating from internal roof damage undergoes a rapid transition from disorder to order. During this stress-release and self-adjustment process, the roof experiences macroscopic progressive instability and deformation, with microseismic events clustering in specific zones, leading to lower fractal dimension values. Once the rock burst concludes and the roof strata stabilize, fractal dimension values increase.

Therefore, spatial variations in the fractal dimension of microseismic energy can serve as a key indicator of the damage evolution process in the roof strata. This effectively reveals the fractal geometric evolution mechanism underlying roof destabilization and confirms the reliability of using the fractal dimension as an early-warning precursor for roof deformation.

Early warning of deformation based on temporal-scale fractal dimensions

The microseismic events along the working face were analyzed by calculating their fractal dimensions on a temporal scale, with particular focus on variations occurring during rock burst events. The sliding-window method used for the spatial analysis was applied to select microseismic events for temporal fractal dimension calculations. Performing equal-time-interval sliding along the time axis and plotting the relationship between the fractal dimension and time yielded the temporal evolution pattern of the microseismic-energy fractal dimension, as shown in Fig. 10.

To validate the stability of the fractal dimension calculation results, this study employed multiple computations with varying window sizes (ranging from 20 m × 20 m × 4 m to 100 m × 100 m × 20 m) and calculated their standard deviations. The results demonstrated that the coefficient of variation for the fractal dimensions under all window sizes was less than 5%, indicating good stability of the computational outcomes.

As shown in Fig. 10a, the fractal dimension exhibits an early-warning period from April 29 to May 3 and a deformation period from May 3 to May 5, indicating that the rock burst is preceded by four days of early warning and two days of deformation. In contrast to conventional mine-pressure monitoring (stress monitoring), the monitoring data surge to 18.3 MPa at the time of the rock burst. As shown in Fig. 10b, the fractal dimension displays an early-warning period from May 28 to June 1 and a deformation period from June 1 to June 4, indicating that the rock burst is preceded by four days of early warning and one day of deformation. In contrast to conventional mine-pressure monitoring (stress monitoring), the monitoring data surge to 21.2 MPa at the time of the rock burst. As presented in Fig. 10c, the fractal dimension exhibits an early-warning period from June 29 to July 3 and a deformation period from July 3 to July 6, indicating that the rock burst is preceded by four days of early warning and two days of deformation. In contrast to conventional mine-pressure monitoring (stress monitoring), the monitoring data surge to 17.1 MPa at the time of the rock burst. As depicted in Fig. 10d, the fractal dimension exhibits an early-warning period from September 21 to September 26 and a deformation period from September 26 to September 30, indicating that the rock burst is preceded by five days of early warning and four days of deformation. In contrast to conventional mine-pressure monitoring (stress monitoring), the monitoring data surge to 22.9 MPa at the time of the rock burst. These results demonstrate that abrupt changes in the fractal dimension precede the corresponding surges in conventional mine-pressure data, suggesting that decreases in the fractal dimension can serve as reliable precursor indicators for the early warning of surrounding-rock deformation.

As illustrated in Fig. 10, the temporal evolution of the fractal dimension during rock bursts can be divided into four distinct stages: stable, early-warning, deformation, and re-stabilization periods. During the stable period, the fractal dimension remains relatively high, generally above 2.5, indicating that microseismic events are in a disordered and discrete state. In the early-warning period, the fractal dimension decreases rapidly, suggesting that microseismic events are transitioning from disorder to order and from dispersion to concentration. During the deformation period, the fractal dimension reaches low values, typically below 1.0. In the re-stabilization period, the fractal dimension increases rapidly, indicating that the energy release caused by damage in the roof strata has been completed and the structure has re-stabilized. The four stages of fractal dimension evolution typically form a dynamic sequence: stable period → early-warning period → deformation period → re-stabilization period, reflecting the core cyclic process of stress accumulation, energy release, and structural equilibrium in the roof strata. Temporal and spatial variations in the fractal dimension of microseismic energy effectively record the energy release process and reveal the underlying failure evolution of the roof strata. Therefore, the fractal dimension of microseismic events is considered to be a meaningful precursor indicator for the early warning of rock bursts.

Conclusion

Based on microseismic monitoring data and the introduction of fractal theory, this study conducted an in-depth analysis of the failure and damage mechanism of surrounding rock preceding rock bursts. It established an early-warning method for rock bursts based on the spatio-temporal evolution of the fractal dimension of microseismic energy. The main contributions and conclusions of this study are as follows:

Theoretical contributions

Established a quantitative relationship between microseismic energy and damage fractal characteristics: Starting from the energy dissipation theory of surrounding rock damage, an integral expression between microseismic energy distribution and fractal dimension was derived and established. This theoretically proves that the seismic

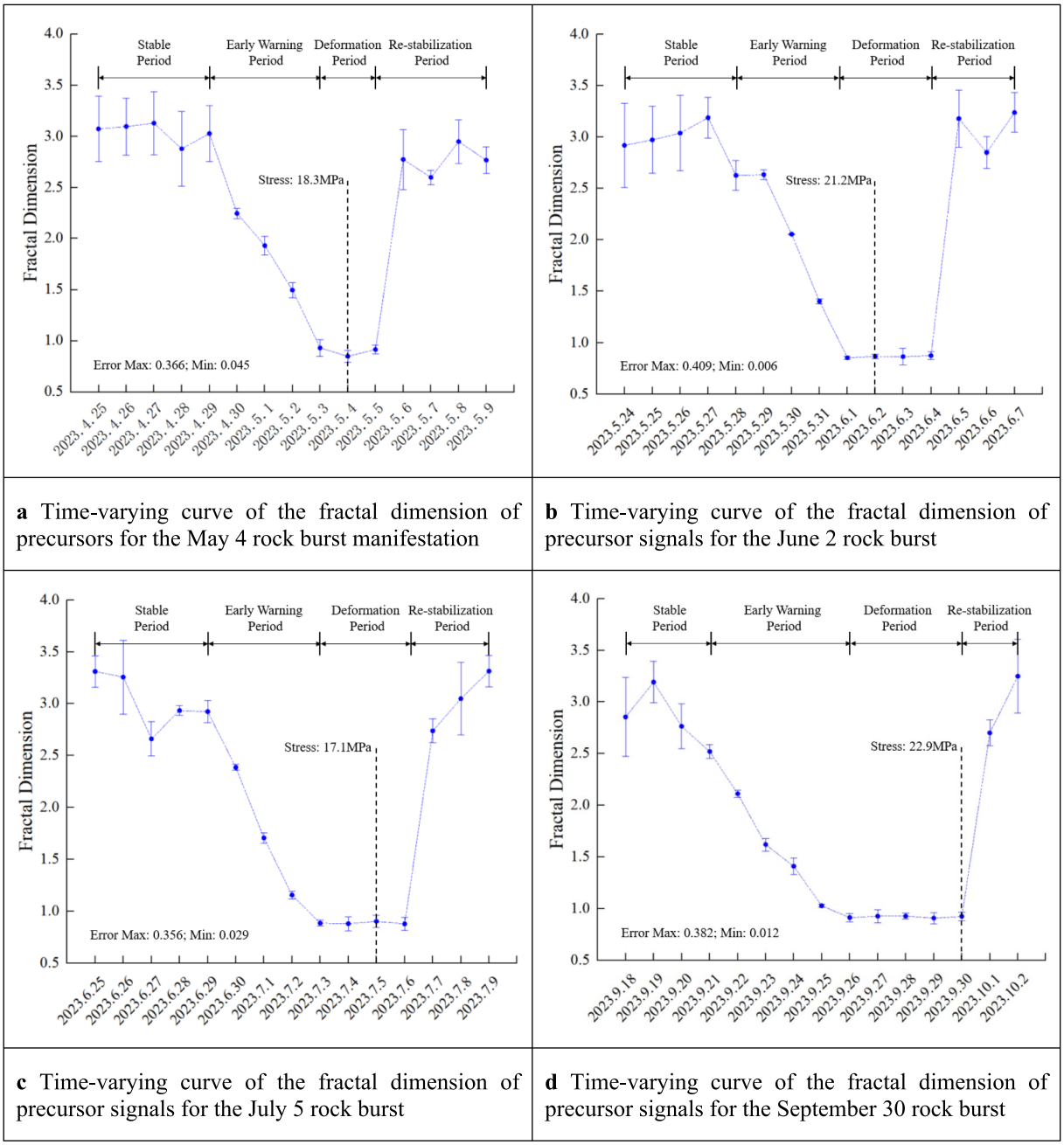

a Time-varying curve of the fractal dimension of precursors for the May 4 rock burst manifestation

b Time-varying curve of the fractal dimension of precursor signals for the June 2 rock burst

c Time-varying curve of the fractal dimension of precursor signals for the July 5 rock burst

d Time-varying curve of the fractal dimension of precursor signals for the September 30 rock burst

Fig. 10. Temporal variation curves of the microseismic-energy fractal dimension.

source energy distribution exhibits fractal characteristics in space, providing a theoretical foundation for using fractal theory to quantitatively describe the damage evolution of rock mass.

Revealed the fractal evolution mechanism of rock burst precursors: The study revealed the physical process before a rock burst where microseismic activity transitions from a disordered, discrete state (high fractal dimension) to an ordered, clustered state (low fractal dimension). It explains the internal mechanism of energy accumulation and release before rock mass instability from the perspective of fractal geometry.

Methodological innovations

Proposed a novel early-warning method based on spatio-temporal evolution of fractal dimension Breaking through the traditional early-warning approach based on statistical parameters like microseismic energy and frequency, this study innovatively proposes an early-warning method using the quantitative indicator “fractal dimension” as the core criterion.

Constructed a four-stage early-warning model based on fractal dimension It clarified that the temporal evolution of the fractal dimension during rock burst manifestations follows a four-stage pattern: "Stable Period → Early

Warning Period→Deformation Period→Re-stabilization Period," providing clear time nodes and criteria for early warning.

Developed a calculation algorithm based on 3D sliding windows A computational method employing 3D sliding window scans along both spatial and temporal axes was adopted, enabling continuous and dynamic calculation of the fractal dimension for microseismic event sets. This enhances the ability to locate risk zones and capture early-warning timing.

Engineering value and application prospects

Provides an earlier warning window Case analysis shows that the decreasing trend of the fractal dimension (Early Warning Period) precedes abrupt changes in conventional stress monitoring data, offering an early warning lead time of up to 3–5 days. This provides valuable time for on-site prevention and control measures.

Potential for integrated engineering application The calculations for this method can be automated based on data from existing microseismic monitoring systems, facilitating integration into intelligent mine comprehensive early-warning platforms. This can form a closed loop of "microseismic monitoring—fractal calculation—automatic early warning," providing a new effective tool for the prevention and control of dynamic disasters in mines.

Limitations

Dependency on sensor network layout The accuracy of the fractal dimension calculation heavily relies on the positioning precision of microseismic events, which is directly constrained by the spatial arrangement of the sensors.

Influence of geological and mining complexity For fractal dimension calculation methods based on microseismic signals, different roof management strategies (such as hydraulic fracturing or roof cutting blasting) can affect the accuracy of microseismic information, potentially influencing the “typical” evolution pattern of the fractal dimension.

Sensitivity to noise and data pre-processing As mentioned in Section "Characterization of microseismic activity" of this paper, the frequency, signal-to-noise ratio (SNR), and spatial filtering thresholds used in data pre-processing rely to some extent on manual experience. Different threshold settings may filter out slightly different event sets, thereby affecting the absolute value of the fractal dimension[13–22].

Data availability

The datasets used and/or analysed during the current study available from the corresponding author on reasonable request.

Received: 24 August 2025; Accepted: 30 September 2025
Published online: 06 November 2025

References

1. Cai, M. et al. Back-analysis of rock mass strength parameters using AE monitoring data. *Int. J. Rock Mech. Min. Sci.* **44**(4), 538–549 (2007).
2. Li, X. L., Chen, S. J., Liu, S. M. & Li, Z. H. AE waveform characteristics of rock mass under uniaxial loading based on Hilbert-Huang transform. *J. Central South Univ.* **28**(6), 1843–1856 (2021).
3. Li, X. L., Chen, S. J., Li, Z. H. & Wang, E. Y. Rockburst mechanism in coal rock with structural surface and the microseismic (MS) and electromagnetic radiation (EMR) response. *Eng. Fail. Anal.* **124**(6), 105396 (2021).
4. Li, X. L. et al. Rock burst monitoring by integrated microseismic and electromagnetic radiation methods. *Rock Mech. Rock Eng.* **49**(11), 4393–4406 (2016).
5. Liu, S. M. et al. Experimental study of effect of liquid nitrogen cold soaking on coal pore structure and fractal characteristics. *Energy* **275**(7), 127470 (2023).
6. Li, H. T. et al. Experimental study on compressive behavior and failure characteristics of imitation steel fiber concrete under uniaxial load imitation steel ffber concrete under uniaxial load. *Constr. Build. Mater.* **399**(8), 132599 (2023).
7. Mandelbrot, B. *Fractal Objects: Form, Opportunity, and Dimension* (World Book Press, 1999).
8. Heping, X. I. E. Fractal geometry and its application in geotechnical mechanics. *J. Geotech. Eng.* **14**(1), 14–24 (1992).
9. Liu, X. & Hou, F. *Chin. J. Rock Mech. Eng.* **S1**, 440–445 (1996).
10. Qian, B. et al. Analysis of surrounding rock damage and deformation warning during excavation of the top arch of the underground powerhouse of Shuangjiangkou hydropower station. *J. Rock Mech. Eng.* **38**(12), 2512–2524 (2019).
11. Mao, H. et al. Rock deformation warning based on microseismic energy fractal dimension. *Tunnel and Underground Engineering Disaster Prevention and Control* (2023).
12. Li, Z. et al. Rockburst occurrences and microseismicity in a longwall panel experiencing frequent rockbursts. *Geosci. J.* **22**, 623–639 (2018).
13. Yu, Y. et al. Research on fractal characteristics of instantaneous microseismic source volume in deep rock mass tunnels. *J. Geotech. Eng.* **39**(12), 2173–2179 (2017).
14. He SQ, Song DZ, Li ZL, et al. Precursor of spatio-temporal evolution law of MS and AE activities for rock burst warning in steeply inclined and extremely thick coal seams under caving mining conditions. Rock Mechanics and Rock Engineering, **2019**, 52(7): 2 415–2 435.
15. Mendecki, A. J. Real time quantitative seismology in mines. *Rock-bursts and Seismicity in Mines* 287–295 (Balkema, 1993).
16. Xu, N. W. et al. Microseismicity and its time–frequency characteristics of the left bank slope at the Jinping First-stage Hydropower Station during reservoir impoundment. *Environ. Earth Sci.* **75**(7), 1–17 (2016).
17. Jiang, P. et al. The relationship between rock mass fracture scale and frequency characteristics and its engineering empirical study. *Geotech. Mech.* **2016**, 483–492 (2016).
18. Rong, H. et al. Quantitative monitoring of underground fault activity and its impact on rockburst. *Coal Sci. Technol.* **52**(2), 10–22 (2024).
19. Cui, F. et al. The spatiotemporal evolution law and induced thrust mechanism of microseismic in complex spatial structure zones of steeply inclined and thick coal seams. *Coal J.* **49**(4), 1786–1803 (2024).

20. Qin, Z. et al. Mechanism and prevention of mining earthquakes in solid coal roadways in deep buried structural areas. *Coal Sci. Technol.* **49**(11), 87–92 (2021).
21. Wang, G. et al. Rockburst mechanism and control in coal seam with both syncline and hard strata. *Saf. Sci.* **115**, 320–328 (2019).
22. Liu, J. P. et al. Studies on temporal and spatial variation of microseismic activities in a deep metal mine. *Int. J. Rock Mech. Min. Sci.* **60**, 171–179 (2013).

Author contributions

ZZJ: Date analysis and theoretical framework. WYl: Literature review and writing. CK: Research plan. LF: Data processing.

Competing interests

The authors declare no competing interests.

Additional information

Correspondence and requests for materials should be addressed to Z.Z.

Reprints and permissions information is available at www.nature.com/reprints.

Publisher's note Springer Nature remains neutral with regard to jurisdictional claims in published maps and institutional affiliations.